HEDL-TME--80-10

DE91 015607

EFFECT OF HEAT TREATMENT AND HEAT-TO-HEAT VARIATIONS IN THE FATIGUE-CRACK GROWTH RESPONSE OF ALLOY 718

PART 2: MICROSCOPIC OBSERVATIONS

Hanford Engineering Development Laboratory

W.J. Mills
L.A. James

April, 1980

DISCLAIMER

This book was prepared as an account of work sponsored by an agency of the United States Government. Neither the United States Government nor any agency thereof, nor any of their employees, makes any warranty, express or implied, or assumes any legal liability or responsibility for the accuracy, completeness, or usefulness of any information, apparatus, product, or process disclosed, or represents that its use would not infringe privately owned rights. Reference herein to any specific commercial product, process, or service by trade name, trademark, manufacturer, or otherwise, does not necessarily constitute or imply its endorsement, recommendation, or favoring by the United States Government or any agency thereof. The views and opinions of authors expressed herein do not necessarily state or reflect those of the United States Government or any agency thereof.

HANFORD ENGINEERING DEVELOPMENT LABORATORY
Operated by Westinghouse Hanford Company
P.O. Box 1970 Richland, WA 99352
A Subsidiary of Westinghouse Electric Corporation
Prepared for the U.S. Department of Energy
under Contract No. DE-AC14-76FF02170

DOE-Richland, WA

DISCLAIMER

HEDL-TME 80-10
UC-79 b,h

EFFECT OF HEAT-TREATMENT AND HEAT-TO-HEAT VARIATIONS IN THE FATIGUE-CRACK GROWTH RESPONSE OF ALLOY 718 — PART 2: MICROSCOPIC OBSERVATIONS

By

William J. Mills and Lee A. James
(AF-15-10-15)

ABSTRACT

The microstructural aspects that influenced the room temperature and elevated temperature fatigue-crack propagation response of annealed, conventional, and modified heat-treated Alloy 718 were studied. Electron fractographic examination of Alloy 718 fatigue fracture surfaces revealed that operative crack growth mechanisms were dependent on heat-treatment, heat-to-heat variations, temperature, and prevailing crack tip stress intensity level. In the low temperature regime (below 538°C), all fracture surfaces exhibited a faceted appearance at low ΔK levels, which is indicative of crystallographic fracture along intense inhomogeneous slip bands. The facets in the modified Alloy 718, however, were found to be rather poorly-defined since the modified heat-treatment tends to promote more homogeneous slip processes. Under progressively higher stress intensity levels, the room temperature and elevated temperature fatigue fracture surfaces exhibited striations, followed by a combination of striations and dimple rupture at the highest ΔK values. Striation spacing measurements in all three heat-treated conditions were generally found to be in agreement with macroscopic growth rates at 24 and 538°C. Under high temperature conditions (above 538°C), evidence of intergranular fracture was also detected on the fatigue fracture surfaces, particularly at low stress intensity levels. This intergranular failure mechanism was found to be more extensive in the modified heat-treated Alloy 718.

CONTENTS

FIGURES

FIGURES (Cont'd)

I. INTRODUCTION

In the companion paper,[1] seven heats of Alloy 718 were fatigue tested at room temperature and elevated temperatures in the conventional, modified, and mill-annealed conditions (see Table 3 of Reference 1). In general, Alloy 718 heats given the modified treatment exhibited superior fatigue resistance when compared to the mill-annealed and conventionally-treated materials. Heat-to-heat variations in fatigue-crack propagation (FCP) rates were observed in conventionally-treated Alloy 718 with Heat A* displaying slightly higher crack growth rates than those exhibited by the other conventional heats. On the other hand, no consistent easily identifiable heat-to-heat variations in FCP behavior were observed in the modified condition.

This portion of the current investigation was undertaken to characterize microstructural aspects of heat-treatment and heat-to-heat variations that influence the FCP response of Alloy 718. Two heats of precipitation heat-treated Alloy 718, Heats A and E, were examined in detail: Heat A was chosen because it exhibited somewhat higher crack growth rates when compared to the other heats of Alloy 718 in the conventional condition; and Heat E was chosen because its cyclic behavior was comparable to that observed in the other heats (Heats B through G) in both the conventional and modified conditions. In addition, microstructural aspects of Heat B given the mill-annealed treatment were also characterized.

As mentioned in the companion paper,[1] Alloy 718 is a metallurgically complex superalloy that involves precipitation of several phases. Accordingly, variations in Alloy 718 precipitation reactions resulting from heat-treatment or heat-to-heat variations could account for the reported differences in FCP behavior. To evaluate this possibility, the effects of heat-treatment and heat-to-heat variations on the microstructure of Alloy 718 Heats A, B, and E were examined by light microscopy and surface replica electron microscopy techniques.

*See Reference 1 for heat identifications, properties, and chemical compositions.

The fatigue fracture surface appearance of metals also provides qualitative as well as quantitative information that is important in determining crack growth mechanisms and post-failure analysis of structural components. Consequently, electron fractographic techniques were employed during this study to develop a comprehensive understanding of room temperature and elevated temperature fatigue fracture mechanisms in Alloy 718 Heats A, B, and E. Operative fracture mechanisms were related to key microstructural features in order to explain the effects of heat-treatment and heat-to-heat variations on the FCP behavior of this nickel-base superalloy. Hence, the work discussed herein summarizes metallographic and fractographic observations of appropriate Alloy 718 fatigue specimens (Heats A, B, and E) tested at temperatures ranging from 24 to 649°C.

II. EXPERIMENTAL PROCEDURE

Metallographic specimens were prepared for optical microscopic examination by using standard metallographic procedures. To reveal the general microstructure, specimens were immersion-etched in 92-ml hydrochloric acid (HCl), 3-ml nitric acid (HNO_3) and rinsed in 90-ml nitric acid (HNO_3) and 45-drops hydrofluoric acid (HF).

Surface replicas were also prepared from metallographic specimens in order to examine the precipitate morphology of heat-treated Alloy 718 in more detail. The surfaces of these samples were mechanically polished and immersion-etched in Tucker's reagent: 45-ml hydrochloric acid (HCl), 15-ml nitric acid (HNO_3), 15-ml hydrofluoric acid (HF) and 25-ml water. Standard two-stage (Pt-Pd-C) replicas were then prepared from the polished surfaces and examined on a Philips EM200 electron microscope operated at an accelerating potential of 60 kV.

To study the fatigue-crack propagation mechanisms operating in Alloy 718, two-stage carbon replicas shadowed parallel to the crack growth direction were made from appropriate fracture surfaces. These replicas were cut into small strips approximately 2 to 3 mm wide. Extreme care was taken in measuring the distance from the crack origin to each strip in an effort to relate the features found on the fracture surface to a corresponding growth rate and ΔK level.

III. RESULTS AND DISCUSSION

A. MICROSTRUCTURE

A summary of the microstructure for Heats A, C, and E is given in Reference 2 and the microstructure for Heat G is given in Reference 3. Typical microstructures for Alloy 718 Heats E and A given the standard and modified heat-treatments are illustrated in Figures 1 and 2. It is obvious from these figures that the higher temperature solution anneal employed in the modified heat-treatment caused considerable grain growth: conventionally-treated Heats A and E had ASTM grain sizes of 11-1/2 and 5, respectively; whereas, modified-treated Heats A and E exhibited grain sizes of 4 and 2-1/2, respectively. Both heats of material exhibited numerous annealing twins and large MC-type carbide inclusions[2] throughout the matrix regardless of heat-treatment. The MC-type carbides were identified by wavelength dispersive X-ray analysis as (Nb,Ti)C.[2]

Conventionally heat-treated Heat E exhibited pronounced banding (note the dark regions in Figure 1a), which usually arises from segregation in the original casting. Surface replication of this material revealed that the banded regions exhibited concentrated Widmanstätten δ precipitates (an orthorhombic Ni_3Nb intermetallic phase) as shown in Figure 3a. Grain boundaries within these banded regions were decorated with a considerable amount of acicular δ particles, while grain boundaries outside the banded regions exhibited only limited evidence of δ precipitates.

When Heat E was given the modified heat-treatment, no evidence of banding was observed optically (Figure 1b), and examination of surface replicas (Figure 3b) revealed no evidence of coarse δ precipitates. The higher solution annealing temperature (1093°C) employed during the modified heat-treatment dissolved the δ phase particles, thereby creating a more homogeneous microstructure. The grain boundaries in the modified material were relatively clean exhibiting only a very fine precipitate structure coupled with a few large carbide inclusions that apparently pinned the grain boundary during the 1093°C solution anneal.

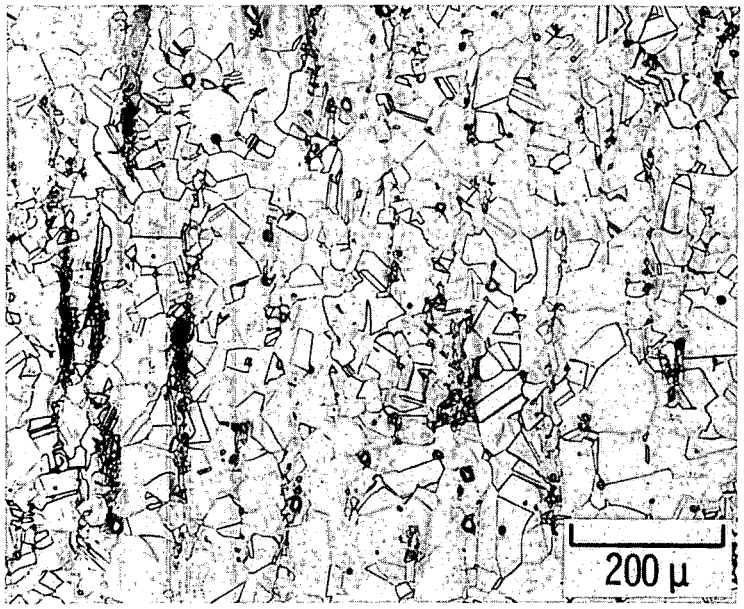

(a)

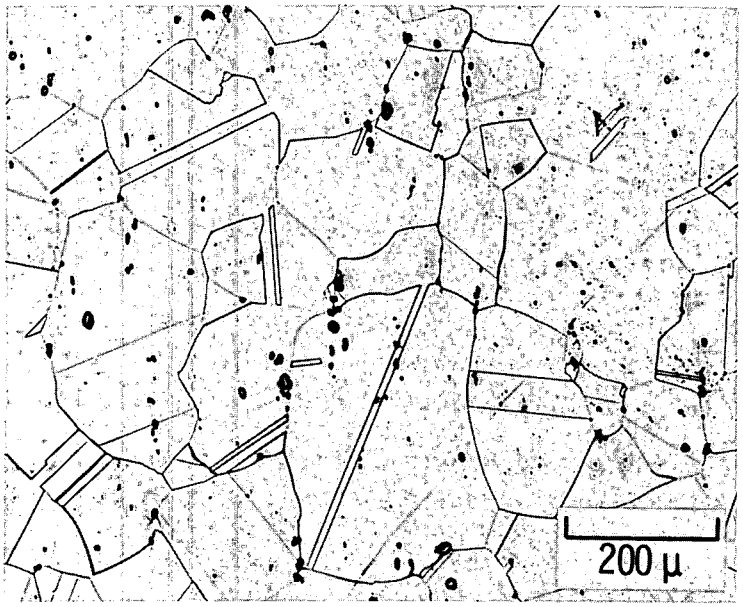

(b)

FIGURE 1. Microstructure of Heat E.
(a) Conventional heat-treatment.
(b) Modified heat-treatment.

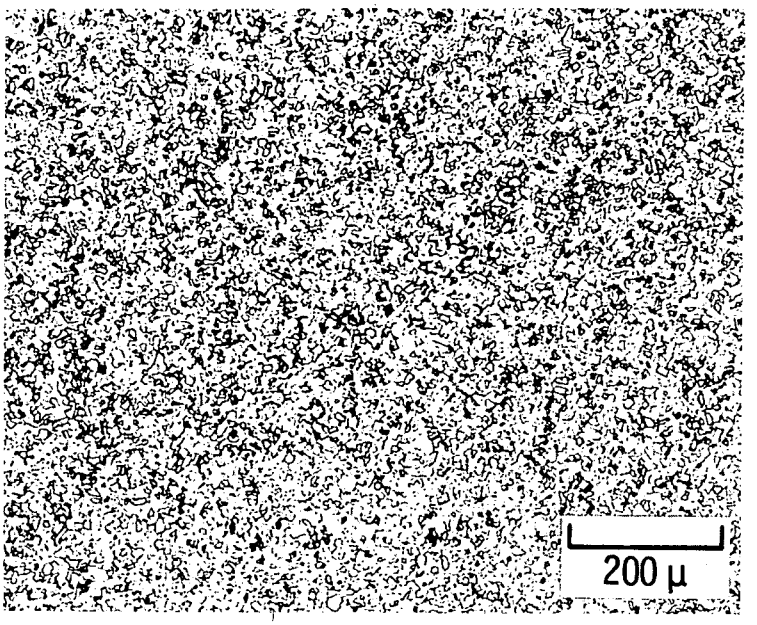

(a)

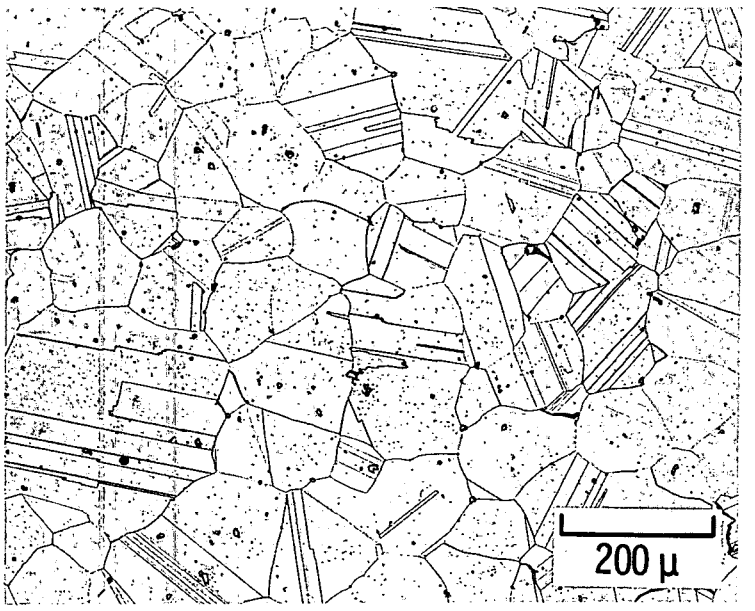

(b)

FIGURE 2. Microstructure of Heat A.
(a) Conventional heat-treatment.
(b) Modified heat-treatment.

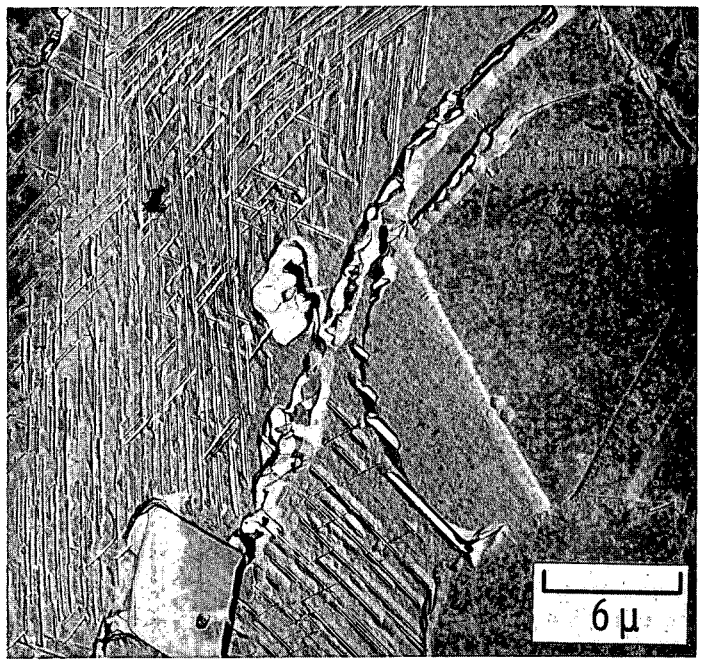

(a)

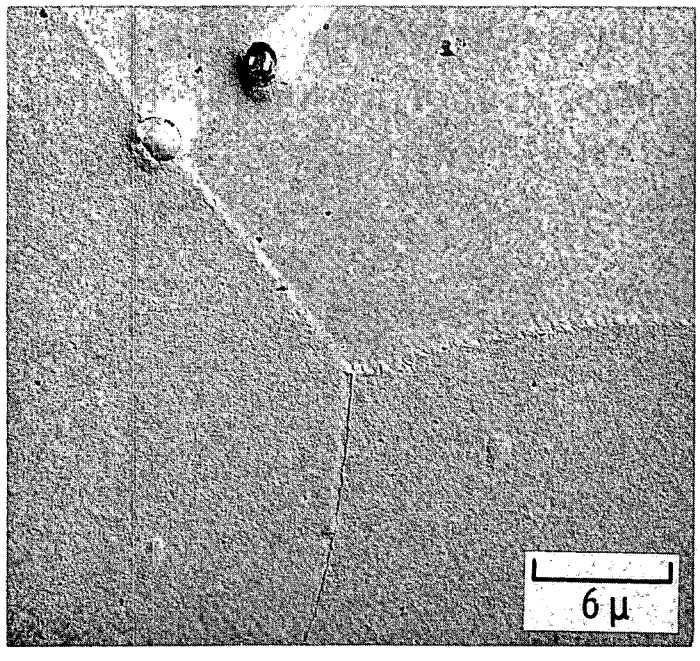

(b)

FIGURE 3. Electron Micrographs of Heat E.
(a) Conventionally heat-treated Alloy 718 with Widmanstätten δ precipitates within banded region. The large inclusions are MC-type carbides.
(b) Modified heat-treated Alloy 718 with a carbide inclusion along the grain boundary.

The typical precipitate morphology for Heat A is illustrated in Figure 4. In the conventionally heat-treated condition (Figure 4a), coarse lenticular δ phase particles were observed along grain boundaries. Intragranular δ precipitates were also detected; however, there was no evidence of δ phase banding as was observed in Heat E. Coarse lenticular δ particles similar to those found in Heat A were also found in conventionally-treated Heats C, F, and G. In summary, coarse δ precipitates were observed in all conventionally-treated heats of Alloy 718 except Heat B. Heat B, however, was solution annealed at 1066°C rather than 954°C prior to receiving the conventional aging treatment. This higher annealing temperature would have dissolved any δ particles originally present, thereby accounting for the absence of δ phase in this heat.

The modified Heat A material (Figure 4b), like the modified Heat E material (Figure 3b), exhibited no evidence of coarse δ particles. Modified-treated Heats C, F, and G were also found to be free of δ precipitates. By way of summary, the microstructures of Heats A, C, E, F, and G given the modified heat-treatment* were found to be essentially the same with each heat exhibiting a coarse grain microstructure, a few MC-type carbides, and no evidence of coarse δ particles. The similar microstructures observed in all modified-treated heats of Alloy 718 account for the lack of any easily identifiable heat-to-heat variations in FCP behavior reported in Reference 1.

The microstructure and precipitate morphology of mill-annealed Heat B are shown in Figures 5 and 6. This heat of material, with an ASTM grain size of 4-1/2, exhibited numerous annealing twins and coarse MC-type carbides throughout the matrix. Grain boundaries were found to be free of second phase precipitates, and no evidence of lenticular δ particles was observed. In all likelihood, the relatively high temperature solution treatment (1066°C) employed during the mill-anneal dissolved any second phase particles that had been present originally.

*Heat B was not tested in the modified condition, and the microstructure of Heat D was not examined.

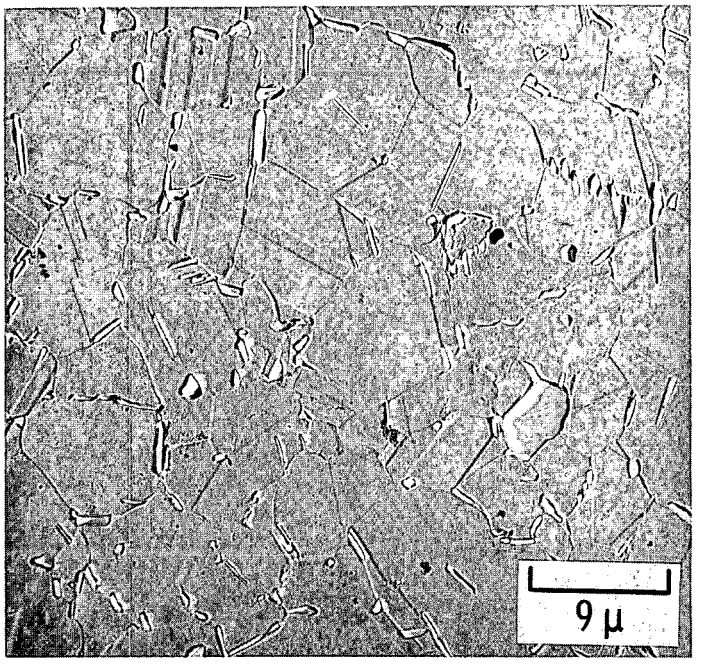

(a)

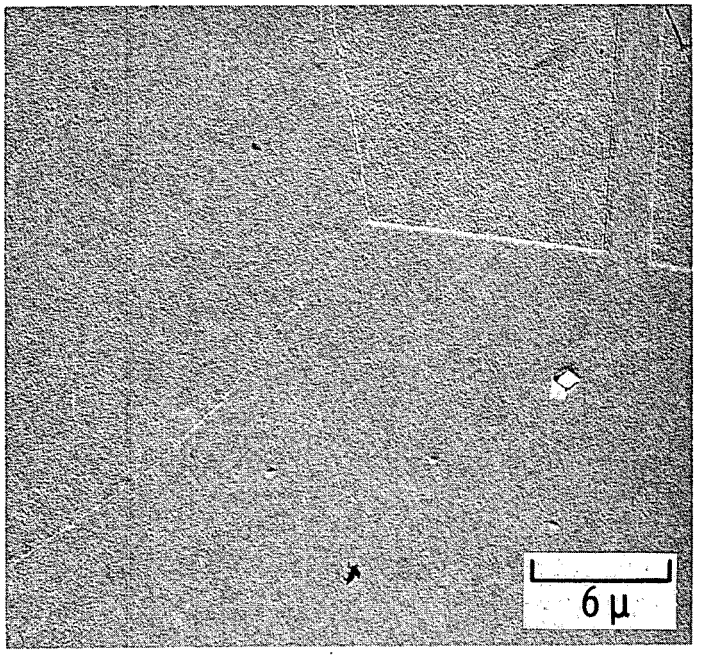

(b)

FIGURE 4. Electron Micrographs of Heat A.
(a) Conventionally heat-treated Alloy 718 with coarse, lenticular δ precipitates.
(b) Modified heat-treated Alloy 718.

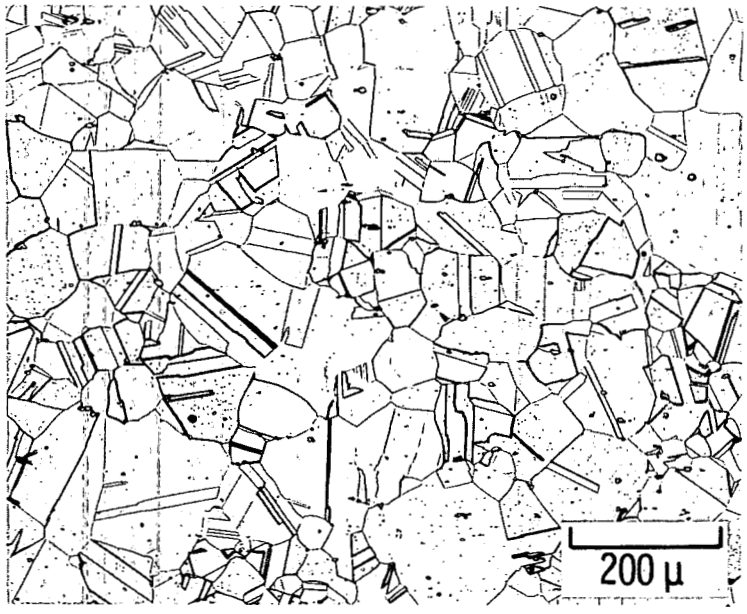

FIGURE 5. Microstructure of Mill-Annealed Heat B.

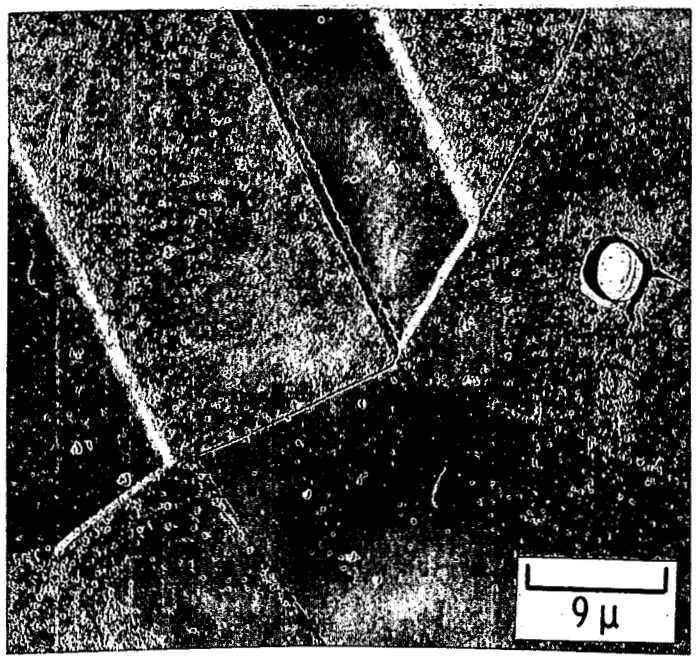

FIGURE 6. Electron Micrograph of Mill-Annealed Heat B with Large Carbide Inclusions.

B. FATIGUE-CRACK PROPAGATION MECHANISMS

Extensive transmission electron fractography of appropriate fatigue fracture surfaces revealed that the FCP mode was primarily transgranular although evidence of intergranular crack growth was observed at test temperatures of 538°C and above. The exact nature of the fatigue fracture surface morphology was found to be dependent on stress intensity factor range, temperature, heat-treatment and heat-to-heat variations. The room temperature and elevated temperature fatigue fracture surface micromorphologies for conventional, modified, and annealed Alloy 718 are discussed in detail in the following three sections.

1. Conventionally Heat-Treated Alloy 718

Typical fracture surface markings for conventionally-treated Alloy 718 Heat E tested at room temperature and intermediate temperatures up to 538°C involved three basic crack growth mechanisms (illustrated in Figure 7), with the operative FCP mechanism being dependent on the magnitude of the prevailing stress intensity factor. At high stress intensity levels associated with rapid FCP rates, fracture surfaces exhibited rather poorly-defined microvoids coupled with large fatigue striations. Under intermediate ΔK levels (approximately 20 to 60 MPa$\sqrt{m}$), fatigue striations were better defined and observed more frequently. The room temperature and elevated temperature microscopic crack growth rates obtained from fatigue striation spacing measurements are compared with macroscopic growth rates as measured with a traveling microscope in Figure 8. These results indicate that microscopic and macroscopic FCP rates for Heat E (represented by circles) were in excellent agreement over a range of ΔK levels from 20 to 70 MPa$\sqrt{m}$. Note that this agreement was observed at both 24 and 538°C. Figure 8 also reveals that striation spacings at both test temperatures were in relatively good agreement with an empirical equation proposed by Bates and Clark:[4]

$$\text{Striation Spacing} \simeq 6 \left(\frac{\Delta K}{E}\right)^2 \qquad (1)$$

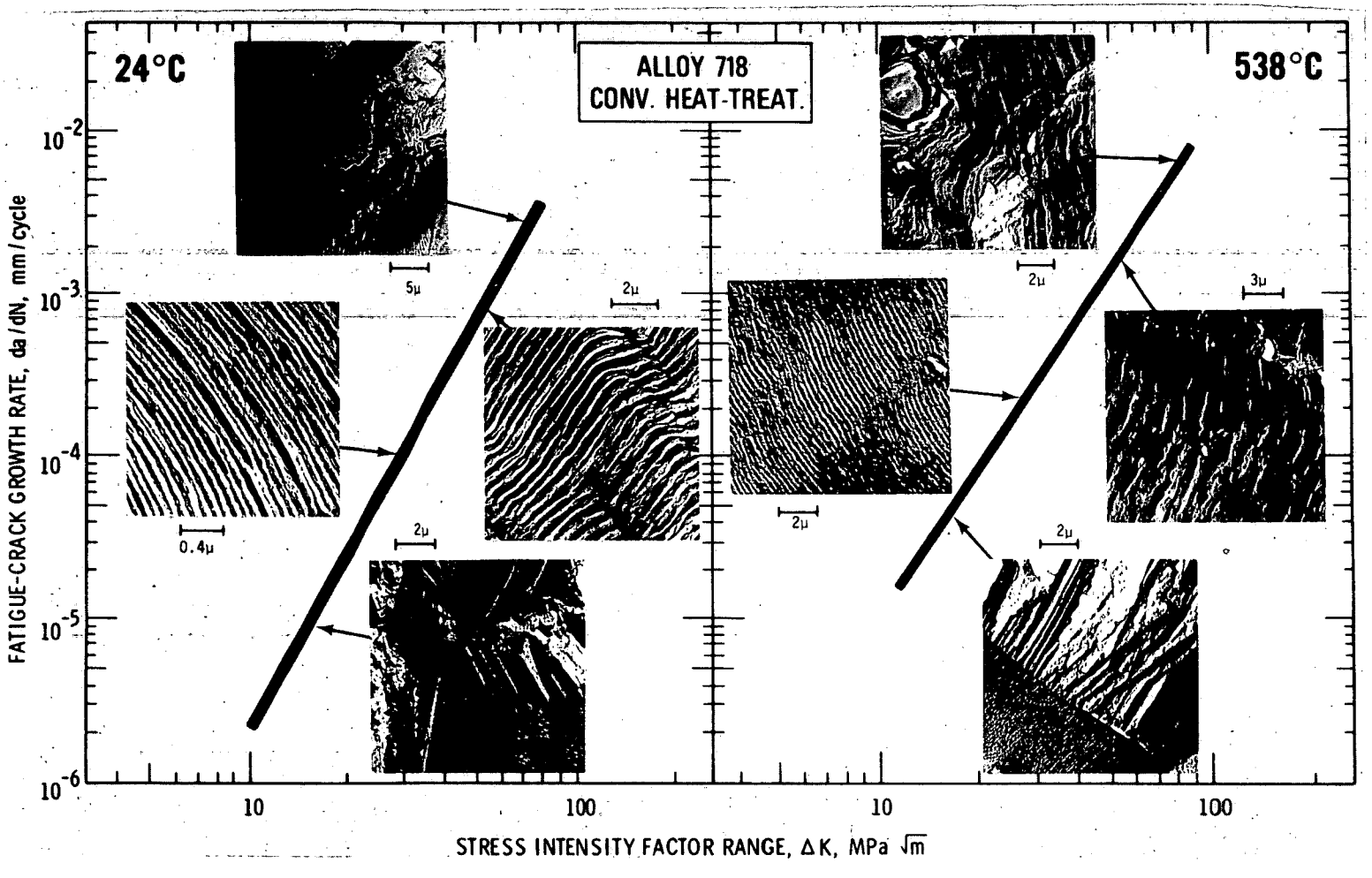

FIGURE 7. Electron Fractographs Illustrating the Room Temperature and 538°C Fatigue Fracture Surface Morphology of Conventional Heat E at Various Positions on the da/dN Versus ΔK Plot. (Neg. 7906409-3)

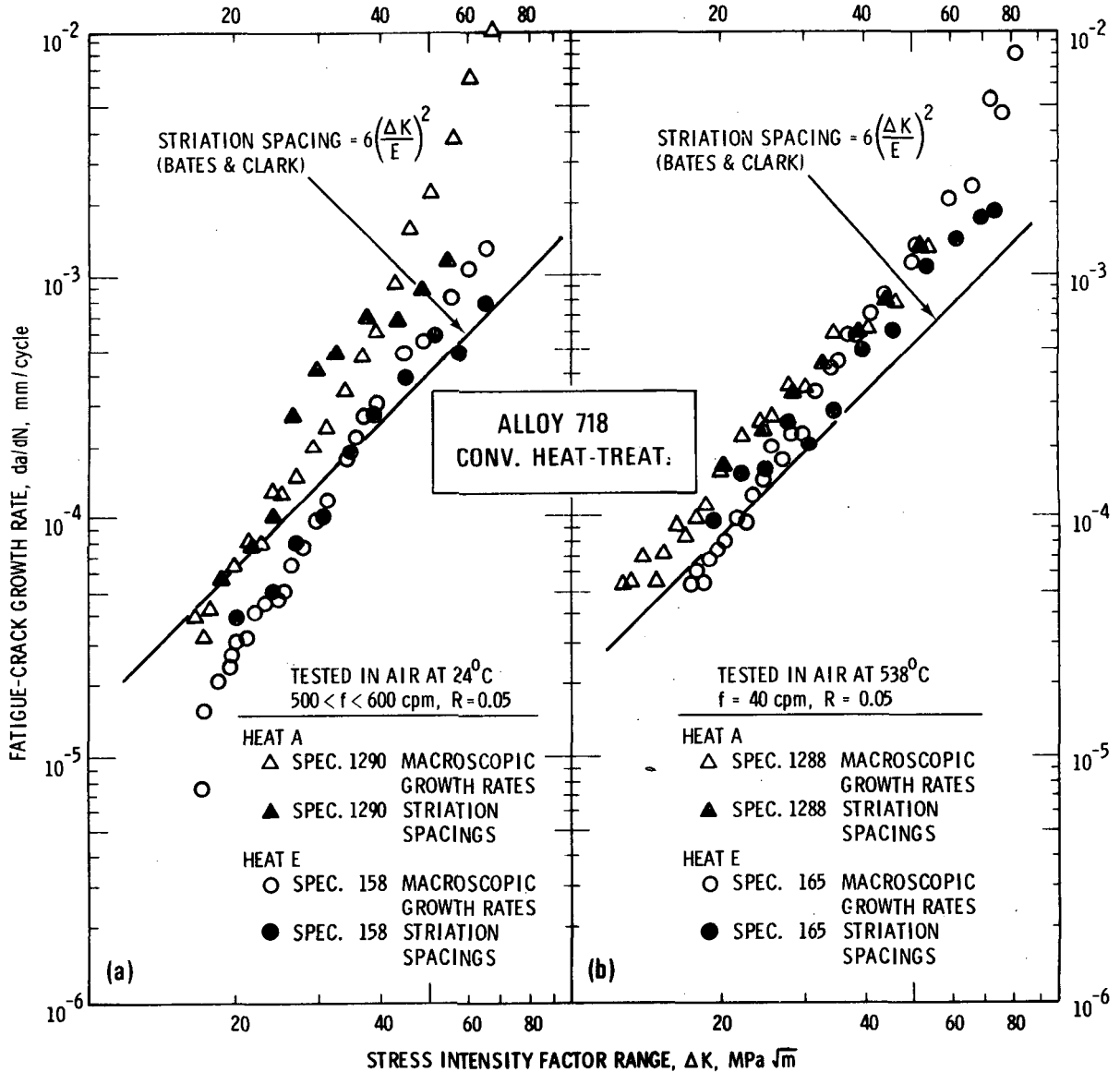

FIGURE 8. Comparison of Striation Spacing Measurements and Macroscopic FCP Rates for Conventionally Heat-Treated Heats A and E at (a) Room Temperature and (b) 538°C. Each solid data point represents an average of approximately 100 striation spacing measurements. (Neg. 7903468-1)

where E represents Young's modulus. The effect of temperature on the Bates and Clark predicted striation spacings was taken into account by choosing an appropriate value of E at each test temperature: at room temperature, E = 200 GPa; and at 538°C, E = 171 GPa.[5]

At progressively lower stress intensity levels (below 20 MPa$\sqrt{m}$), fracture surfaces took on a highly faceted or cleavage-like appearance, indicative of the crystallographic fracture along intense, heterogeneous deformation bands. Similar faceted growth mechanisms were reported previously in numerous nickel-base alloys at low crack growth rates.[6-16] Parallel markings were often superimposed on the crystallographic facets as shown in Figure 9a. These fine, straight lines were found to be much more uniform and more evenly spaced (approximately 25 nm) than classic fatigue striations. Furthermore, when these parallel markings and fatigue striations appeared in the same region (Figure 9b), the striation spacing was consistently greater than the spacing of the straight lines. These observations suggest that the parallel markings represent slip offsets produced by the severe stresses present in the wake of the crack front. In support of this hypothesis, thin foil studies of Alloy 718 fatigue fracture surfaces by Clavel and Pineau[14] revealed the presence of inhomogeneous plastic deformation bands (both slip bands and deformation twins) near the fatigue fracture surface. The slip band spacing (approximately 50 to 150 nm), as measured from thin foil micrographs in Reference 12, was found to be within an order of magnitude of the spacing between parallel fracture surface markings (25 nm), which provides additional evidence that these fine lines superimposed on crystallographic facets represent slip offsets.

At the highest test temperature (649°C), a transgranular-to-intergranular fracture mechanism transition was observed. Under intermediate and high stress intensity factor conditions, the fatigue fracture surface of conventional Heat E was predominately transgranular exhibiting evidence of fatigue striations (Figure 10a) similar to that observed at room temperature and intermediate temperatures. At lower ΔK levels, however, the fracture surface took on an intergranular appearance (as shown in Figure 10b), in contrast to

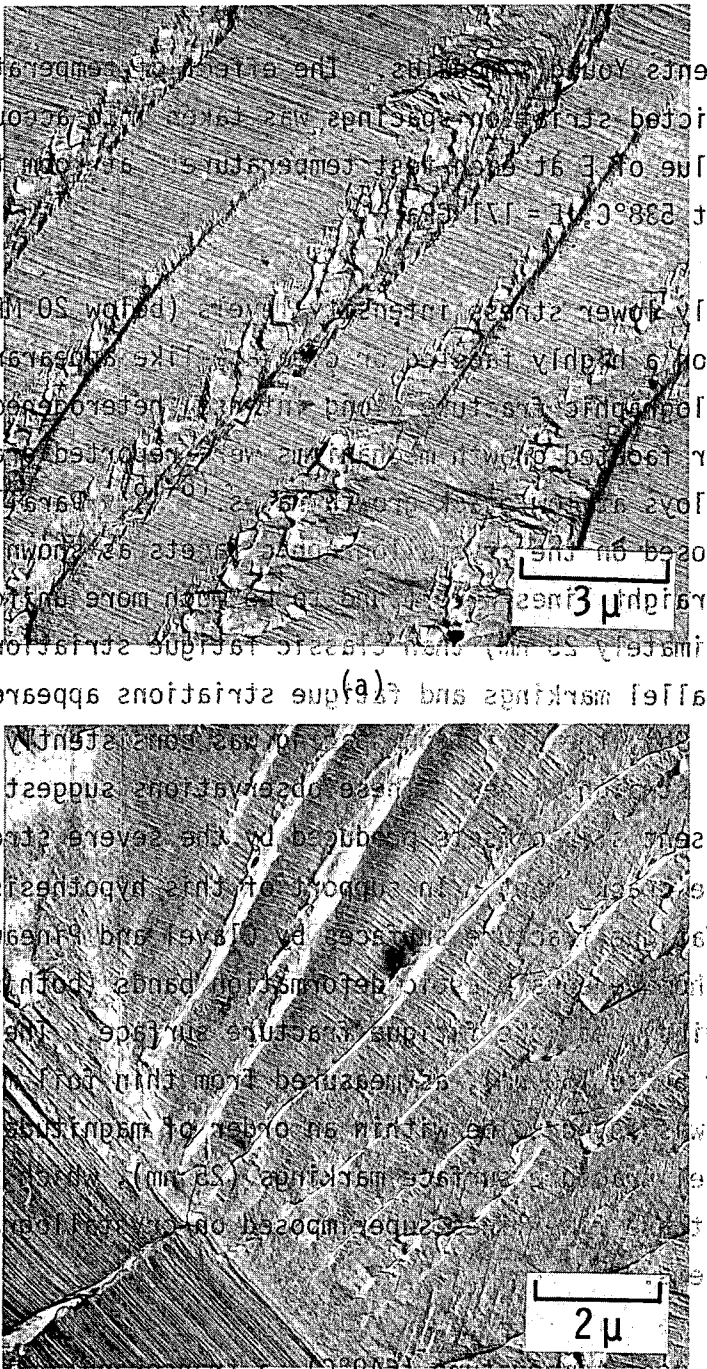

FIGURE 9. Electron Fractographs of Conventional Alloy 718 Under Low ΔK Conditions.
(a) Parallel fracture markings superimposed on crystallographic facets.
(b) Fine lines (lower left-hand corner) and fatigue striations. Note that striation spacings were approximately twice the spacing of the fine lines (40 versus 22 nm).

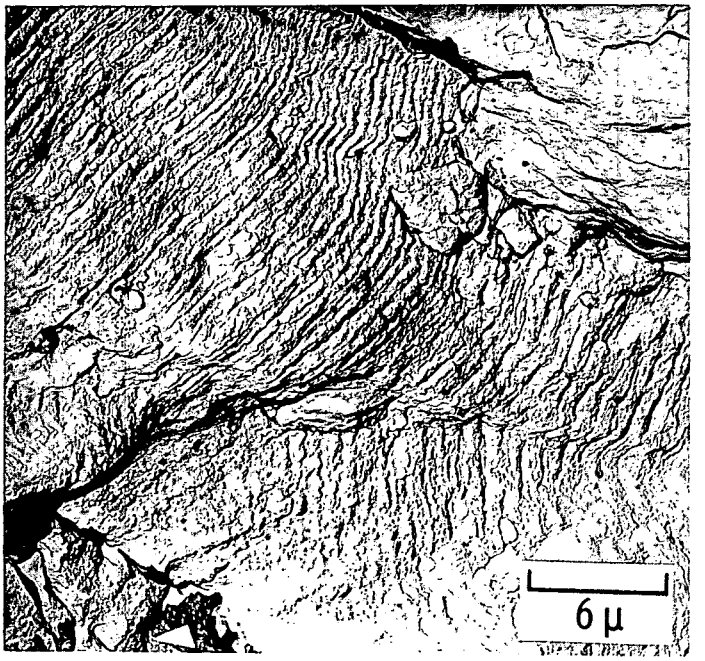

(a)

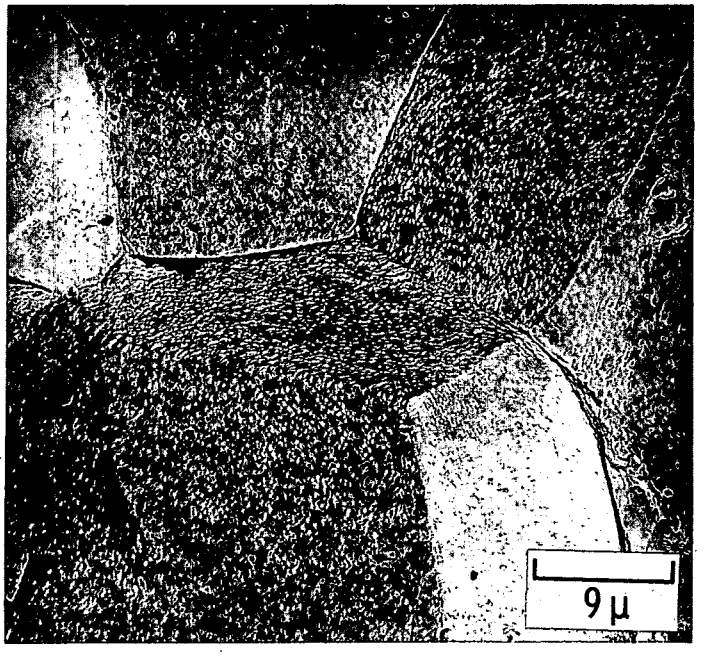

(b)

FIGURE 10. Fracture Surface Appearance of Conventionally Heat-Treated Alloy 718 at 649°C.
(a) Fatigue striations observed under intermediate ΔK conditions.
(b) Intergranular fracture observed in the low ΔK regime.

the transgranular faceted growth mechanism observed at lower temperatures (Figure 7).

Typical fatigue fracture markings for conventional Heat A tested at temperatures ranging from 24 to 538°C are shown in Figure 11. In general, the fracture surface morphology for this heat was rather similar to that of conventional Heat E (Figure 7) except for one feature, additional evidence of dimple rupture. Under high ΔK conditions, Heat A fracture surfaces were completely covered with well-defined dimples (Figure 11a), in contrast to the rather poorly-defined dimples and large striations observed in Heat E under comparable ΔK levels. Furthermore, in Heat A evidence of dimple rupture coupled with relatively small patches of fatigue striations persisted at intermediate and low stress intensity levels as shown in Figures 11b and 11c, respectively. No evidence of dimple rupture was observed in Heat E under these conditions.

Figures 11b and 11c also reveal that striations tend to curve around dimples (i.e., striations are oriented in various directions irrespective of the overall crack growth direction). This finding indicates that microvoids nucleated ahead of the macroscopic crack front. More specifically, these microvoids initiated dimple rupture beyond the advancing crack tip and crack extension between the dimples then occurred by a striation formation mechanism, which accounts for striations being oriented in various directions. A particularly good example of this behavior is illustrated between the two arrows in Figure 11b. In this region, a series of coarse, lenticular δ phase particles separated from the matrix and formed an elongated dimple ahead of the advancing crack front. (Note the lenticular δ precipitates on the fracture surface in Figure 11b.) The fatigue crack then propagated into the surrounding material in a cyclic manner as indicated by the striations being parallel to the elongated dimple even though this orientation is normal to the overall macroscopic crack front.

Striation spacings and macroscopic FCP rates for conventionally-treated Heat A are compared in Figure 8. Under room temperature conditions, microscopic

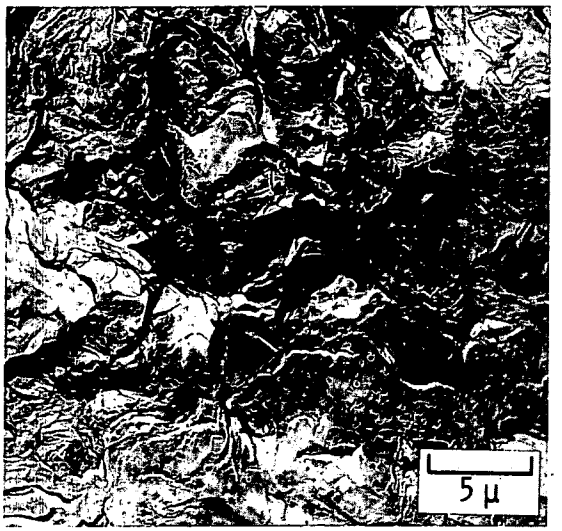

(a)

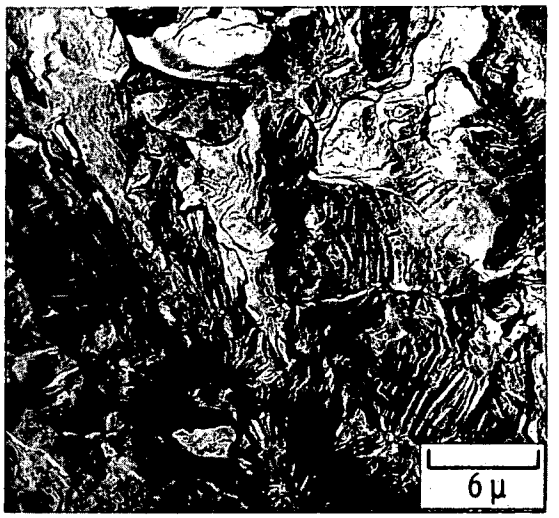

(b)

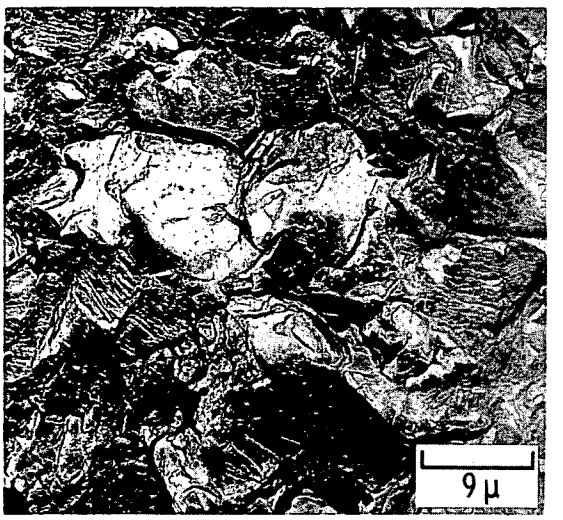

(c)

FIGURE 11. Electron Fractographs Illustrating the Fracture Surface Morphology of Conventional Heat A.
(a) Extensive dimple rupture found at high FCP rates at room temperature.
(b) Dimple rupture coupled with striations observed under intermediate growth rates at room temperature. Arrows denote a row of lenticular δ particles on the fracture surface.
(c) Dimple rupture and fatigue striation found at 538°C.

and macroscopic crack growth rates were in good agreement at intermediate ΔK levels (20 to 50 MPa$\sqrt{m}$). This agreement between striation spacings and macroscopic FCP data indicates that striation formation in the matrix controlled the fatigue response of Heat A under intermediate ΔK levels even though considerable evidence of dimple rupture was observed in this regime (recall Figure 11b). Figure 8 also reveals that striation spacings for Heat A were somewhat larger than those in Heat E at a given ΔK level, which accounts for the slightly higher FCP rates observed in Heat A under intermediate stress intensity conditions. At higher ΔK levels (50 to 60 MPa$\sqrt{m}$), striation spacings in Heat A were approximately a factor of 3 lower than macroscopic FCP rates. This difference, coupled with the observation that dimples dominated the fracture surface at high crack growth rates (Figure 11a), indicates that the dimple rupture mechanism rather than striation formation controlled the room temperature fatigue response of Heat A under high ΔK conditions. Furthermore, this increased dimple rupture observed at high FCP rates accounts for the acceleration in macroscopic growth rates and the significant discrepancy in fatigue behavior between Heats A and E in the high ΔK regime at room temperature.

At 538°C microscopic and macroscopic growth rates for conventional Heat A were found to be in excellent agreement (Figure 8b). In addition, striation spacings for Heat A agreed very well with those measured in Heat E, which is consistent with the comparable macroscopic crack growth rates exhibited by Heats A and E at this test temperature. Finally, Figure 8 reveals that experimentally determined striation spacings for Heat A tend to fall slightly above the Bates and Clark empirical relationship (Equation (1)) at both room temperature and 538°C.

In the 649°C regime, the conventional Heat A fracture surface exhibited considerable intergranular fracture under all stress intensity levels, in contrast to Heat E where intergranular failure was confined to low ΔK levels (Figure 10). This increased intergranular cracking coupled with the large amount of grain boundary surface area in Heat A (recall that conventionally-treated Heat A exhibited a very fine grain size of 11-1/2) are believed to be

responsible for the inferior FCP response of this Alloy 718 heat at 649°C (see Figure 5 in Reference 1).

2. Modified Heat-Treated Alloy 718

The fatigue fracture surface morphologies of modified Heats A and E were found to be very similar at all test temperatures. Typical fracture surface markings for modified Alloy 718 at 24 and 538°C are summarized in Figure 12. In the low ΔK regime, Figure 12 reveals that faceted growth behavior was dominant at room temperature, whereas extensive intergranular fracture was observed at 538°C. Under progressively higher stress intensity conditions, both the room temperature and 538°C fatigue fracture surfaces exhibited fatigue fissures and striations followed by a duplex mechanism involving microvoid coalescence and striation formation in the highest ΔK regime. At the highest test temperature (649°C), extensive intergranular fracture was observed under both low and intermediate stress intensity conditions (Figure 13a), while a combination of intergranular fracture coupled with limited evidence of striation formation (Figure 13b) was found at higher ΔK values (40 to 50 MPa$\sqrt{m}$).

Striation spacings and macroscopic FCP rates for the modified Heats A and E were compared at room temperature and 538°C (Figure 14). Before examining this figure, however, it is important to note that the extensive amounts of fissures (Figure 12) coupled with ill-defined striations made it extremely difficult to obtain accurate spacing measurements, especially at room temperature. Consequently, the results plotted in Figure 14 were obtained by careful measurement of many very small patches of fatigue striations (each solid data point represents approximately 90 striation spacing measurements) which actually comprise a rather low percentage of the total fracture surface. Nevertheless, the room temperature microscopic and macroscopic FCP rates were found to be in good agreement at ΔK levels above 30 MPa$\sqrt{m}$; striation spacing measurements were slightly greater than macroscopic values at ΔK levels below 30 MPa$\sqrt{m}$. Figure 14a also reveals that experimentally determined striation spacings for Heat A were consistent with the Bates and Clark

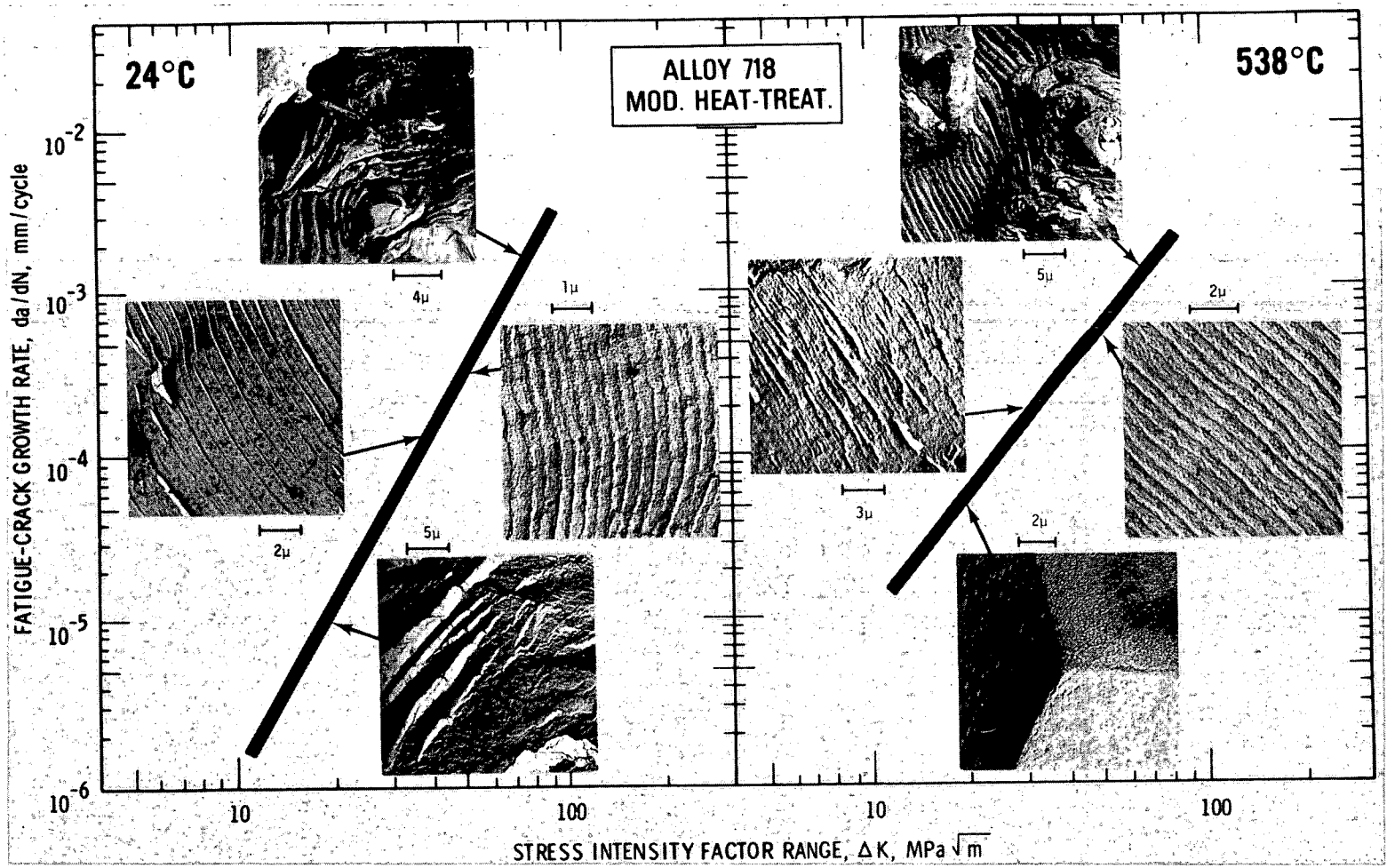

FIGURE 12. Electron Fractographs Illustrating the Fatigue Fracture Surface Appearance of Modified Heat-Treated Alloy 718 Under Various FCP Rates at 24 and 538°C. (Neg. 7906409-1)

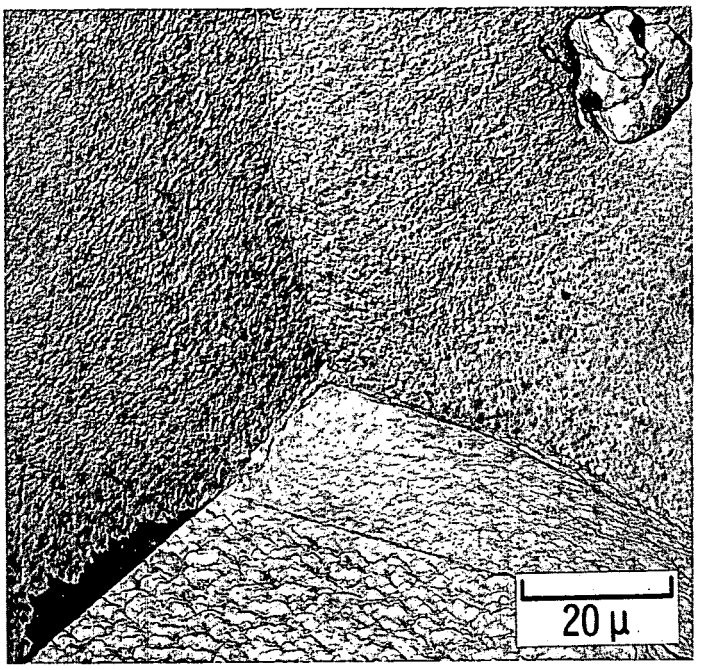

(a)

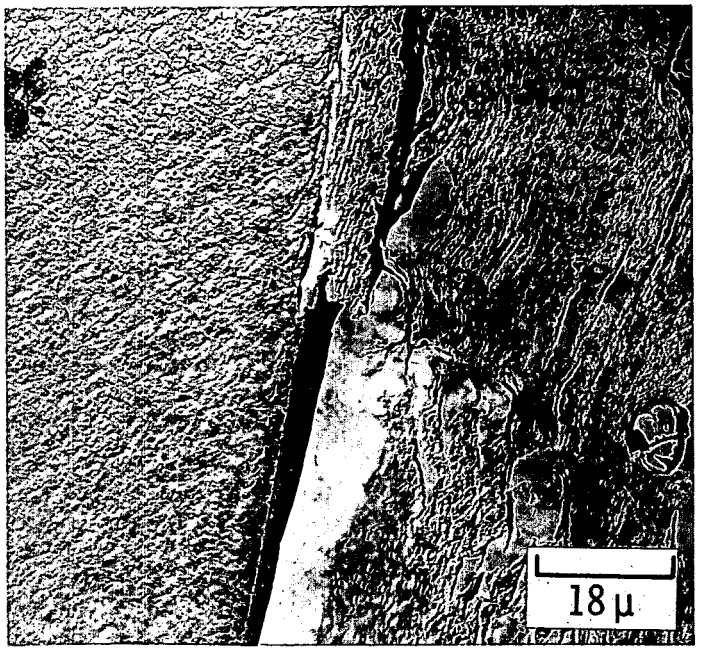

(b)

FIGURE 13. Electron Fractographs Illustrating Fatigue Fracture Surface Appearance of Modified Alloy 718 at 649°C.
(a) Intergranular fracture at ΔK levels below 40 MPa$\sqrt{m}$.
(b) Combination of intergranular cracking (left side of fractograph) and striation formation at ΔK levels above 40 MPa$\sqrt{m}$.

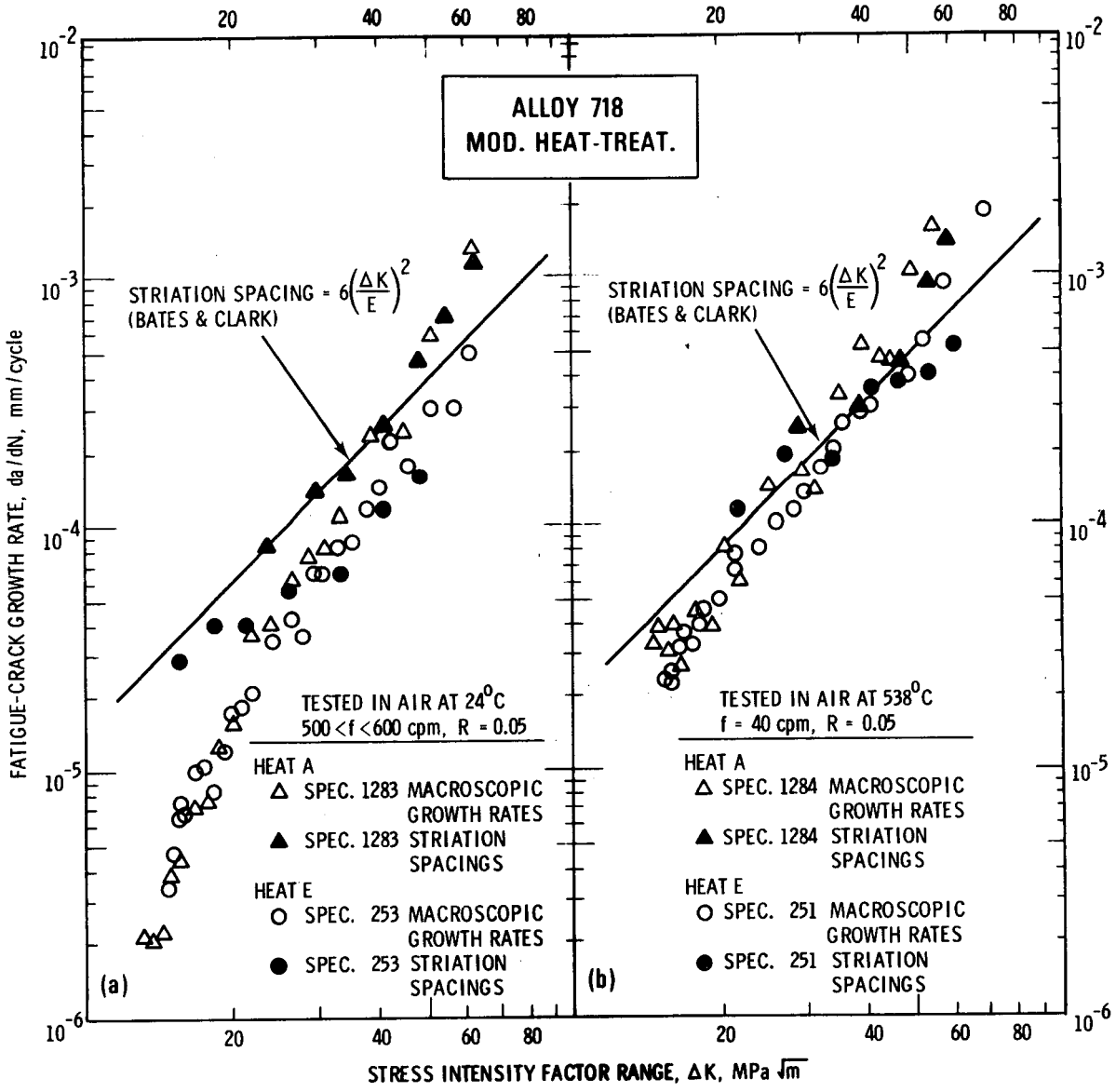

FIGURE 14. Comparison of Striation Spacing Measurements and Macroscopic Crack Growth Rates for Modified Heat-Treated Heats A and E at (a) Room Temperature and (b) 538°C. Each solid data point represents an average of approximately 90 striation spacing measurements. (Neg. 7903468-2)

empirical relationship (Equation (1)), whereas microscopic growth rates in Heat E tend to fall slightly below the Bates and Clark equation under room temperature conditions. At 538°C striation spacing measurements for both heats of modified Alloy 718 were found to be in excellent agreement with both macroscopic FCP rates as well as the Bates and Clark equation.

In general, the fracture surface appearance of the modified Alloy 718 (Figures 12 and 13) was rather similar to fracture markings observed in the conventional material (Figure 7), but a few interesting differences were also noted. For example, in contrast to the crisp cleavage-like facets found in conventionally-treated Alloy 718 (Figure 7), the faceted appearance exhibited by the modified material was rather poorly-defined (Figure 12), which suggests that plastic deformation was not confined to intense, narrow bands of slip planes in the modified material. In addition, the fine slip offsets superimposed on the crystallographic facets in the conventional condition were not observed in the modified condition. This lack of intense slip offsets on the modified fatigue fracture surfaces further suggests that slip tended to be more homogeneous in the modified superalloy. These observations are consistent with Smith and Michel's findings[17] that the modified heat-treatment coarsens the γ'' precipitates which promotes homogeneous deformation since the larger precipitates are more resistant to dislocation shearing.

Under intermediate FCP rate conditions (approximately 10^{-4} mm/cycle), the modified-treated fracture surfaces were covered with fatigue fissures (Figure 12), rather than the well-defined fatigue striations exhibited by the conventional material (Figure 7). The abundance of fissures made it extremely difficult to find individual striations, especially at room temperature. At higher temperatures (up to 538°C), small regions of well-defined striations were observed although fatigue fissures still dominated the fracture surface.

Both heat-treatments resulted in considerable intergranular failure at 649°C (Figures 10 and 13); however, the modified-treated Alloy 718 exhibited intergranular fracture at 538°C in the low ΔK regime (Figure 12), whereas the conventional Alloy 718 exhibited transgranular faceting under these conditions.

This phenomenon is believed to be related to the difference in grain size for the two heat-treatments. Recall that the modified solution anneal results in the formation of very large grains as shown in Figures 1b and 2b. In a previous study of the elevated temperature FCP response of Alloy 718, Clavel and Pineau[14] reported that intergranular cracking occurred preferentially along the boundaries of larger grains. Based on this observation, the material given the modified heat-treatment would be expected to exhibit additional intergranular fracture which is consistent with experimental results obtained during the current investigation.

Although a number of differences were noted in the conventional and modified fracture surface markings, the exact cause of the slightly improved fatigue resistance exhibited by the modified Alloy 718 is still not completely understood. Nevertheless, possible explanations for this phenomenon are suggested below. In a previous study, Smith and Michel[17] attributed the improved FCP response of modified Alloy 718 to enhanced homogeneous slip processes that resulted from coarsening of γ'' precipitates during the modified heat-treatment. The ill-defined facets observed in the modified material at low FCP rates (Figure 12), in marked contrast to the well-defined crystallographic facets found in the conventional Alloy 718 (Figure 7), support this hypothesis under low stress intensity conditions. In the intermediate and high ΔK regimes, however, the presence of striations on conventional and modified fracture surfaces indicates that homogeneous slip was prevalent in both heat-treated conditions. In essence, the enhanced homogeneous slip process exhibited by the modified material appears to explain the improved fatigue behavior at low stress intensity conditions; however, this argument is suspect at higher ΔK levels.

In another study, Mills and James[16] suggested that the absence of coarse δ particles in the modified microstructure provided greater resistance to fatigue-crack extension. Recall that the coarse δ phase network found throughout conventional Heat A initiated extensive dimple rupture (Figure 11a), thereby resulting in a significant acceleration in crack growth rates under high ΔK conditions (see Figure 1 in Reference 1). When this heat was given

the modified heat-treatment, which dissolved the coarse δ particles (Figure 4b), no acceleration in crack growth rates was detected. Hence, the dissolution of δ precipitates during the modified treatment appears to improve the fatigue response of Alloy 718 under high ΔK conditions; however, this argument is also suspect in the intermediate stress intensity regime. Under intermediate growth rates, striation spacings and macroscopic FCP rates for conventional Alloy 718 were in excellent agreement (Figure 11), indicating that striation formation, rather than dimple rupture, controlled the fatigue response of the conventional superalloy. Consequently, even though the δ particles initiated dimples ahead of the advancing crack front at intermediate ΔK levels (as illustrated in Figures 10b and 10c), they did not influence the overall macroscopic FCP rates in this regime.

At intermediate crack growth rates, the only discernible differences between the conventional and modified fracture surfaces were slightly smaller striation spacings at a given ΔK level and increased evidence of fatigue fissures in the modified material. These observations suggest that the modified matrix was more resistant to striation formation, which would account for the somewhat lower FCP rates exhibited by the modified Alloy 718.

3. Annealed Alloy 718

The fatigue fracture surface appearance of annealed Heat B at 24 and 538°C (illustrated in Figure 15) was found to be very similar to that of conventionally-treated Alloy 718 (Figure 7). Like the conventional material, the annealed Alloy 718 exhibited three basic crack growth mechanisms at each test temperature, with the operative mechanism being dependent on the applied stress intensity range. Under high ΔK conditions (above 50 MPa$\sqrt{m}$), a duplex process was observed involving fatigue striations and microvoids initiated by broken MC-type carbides. In the intermediate stress intensity regime (20 to 50 MPa$\sqrt{m}$), well-defined striations covered the fracture surface, although numerous broken carbides were also found. By back-counting the striations in the vicinity of these carbide inclusions (Figure 16), it is seen that the particles failed as the crack front reached

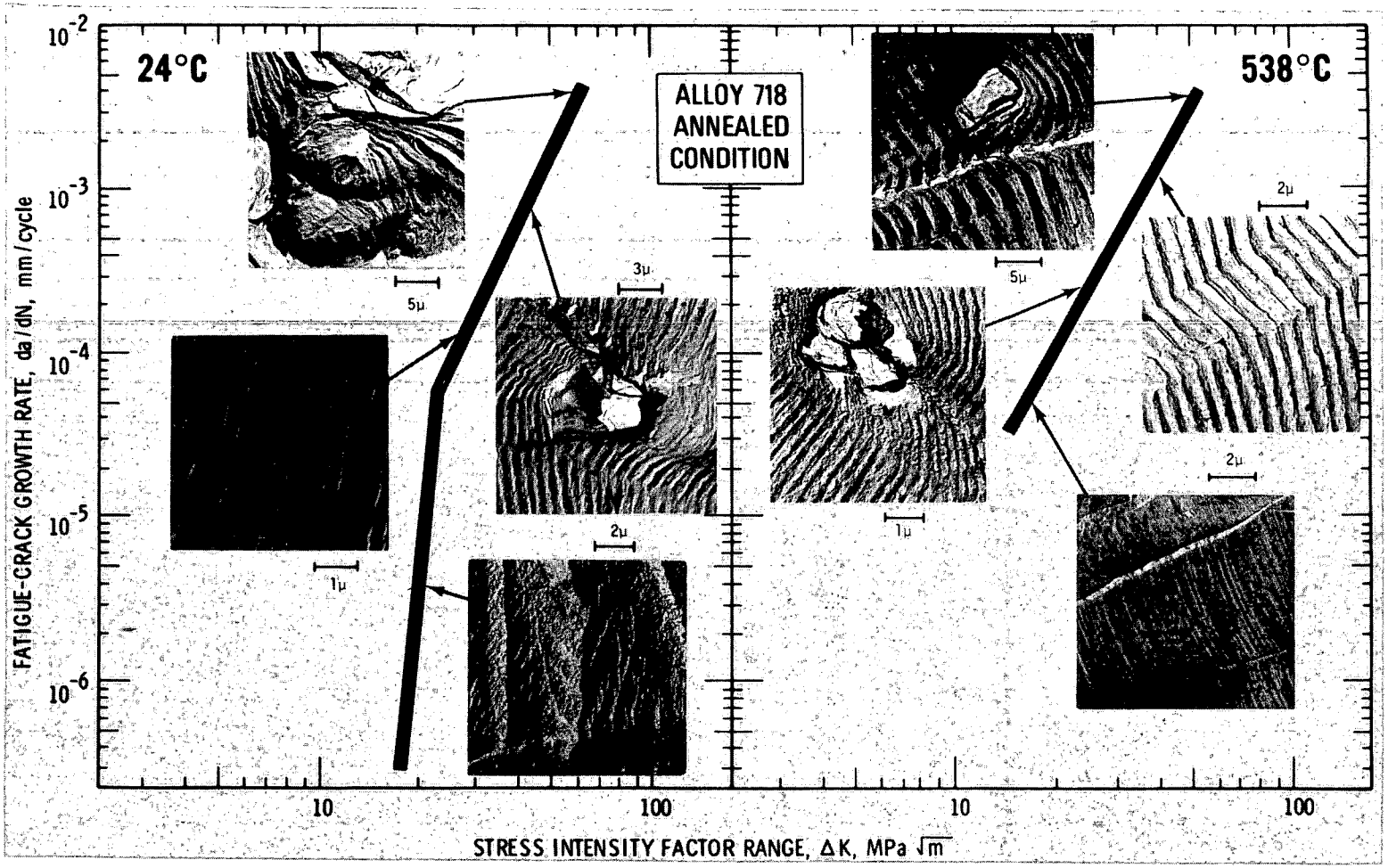

FIGURE 15. Electron Fractographs Illustrating the Room Temperature and 538°C Fatigue Fracture Surface Morphology of Annealed Alloy 718 at Various Positions on the da/dN Versus ΔK Plot. (Neg. 7906409-2)

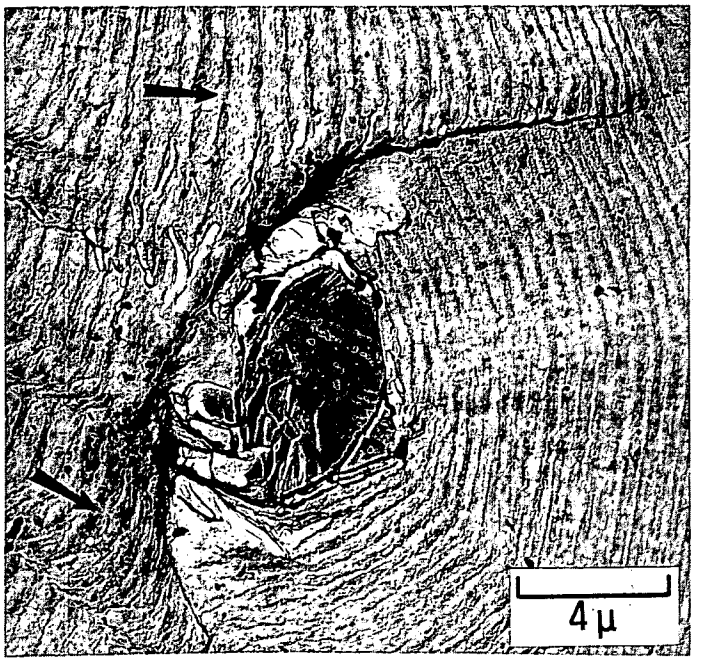

FIGURE 16. Electron Fractograph of Annealed Alloy 718 Revealing a Broken MC-Type Carbide Inclusion Surrounded by Fatigue Striations. Arrows denote position of crack front when the inclusion failed.

the inclusions, rather than failing ahead of the advancing crack front. Figure 16 also reveals that localized accelerations in FCP rates caused by these broken particles were compensated for by the formation of smaller striations in the wake of the inclusion until the localized crack front finally joined up with the overall advancing crack tip.

Striation spacings and macroscopic crack growth rates in the annealed Alloy 718 were found to be in excellent agreement at 24 and 538°C as indicated in Figure 17. On the other hand, striation spacing measurements deviated from the empirical Bates and Clark equation (Equation (1)), particularly at higher FCP rates. In fact, for a measured striation spacing of 10^{-3} mm, the Bates and Clark equation overestimated ΔK by approximately 70% at room temperature and 538°C.

In the low stress intensity regime (below 20 MPa$\sqrt{m}$), the annealed Alloy 718, like the conventional material, exhibited a well-defined faceted appearance (Figure 15). In addition, periodic slip offsets were often superimposed on the crystallographic facets of annealed Heat B at 24 and 538°C. The spacing of these fine, straight lines (approximately 30 to 50 nm) was found to be slightly larger than the spacing of parallel fracture markings in conventional Alloy 718 (25 nm).

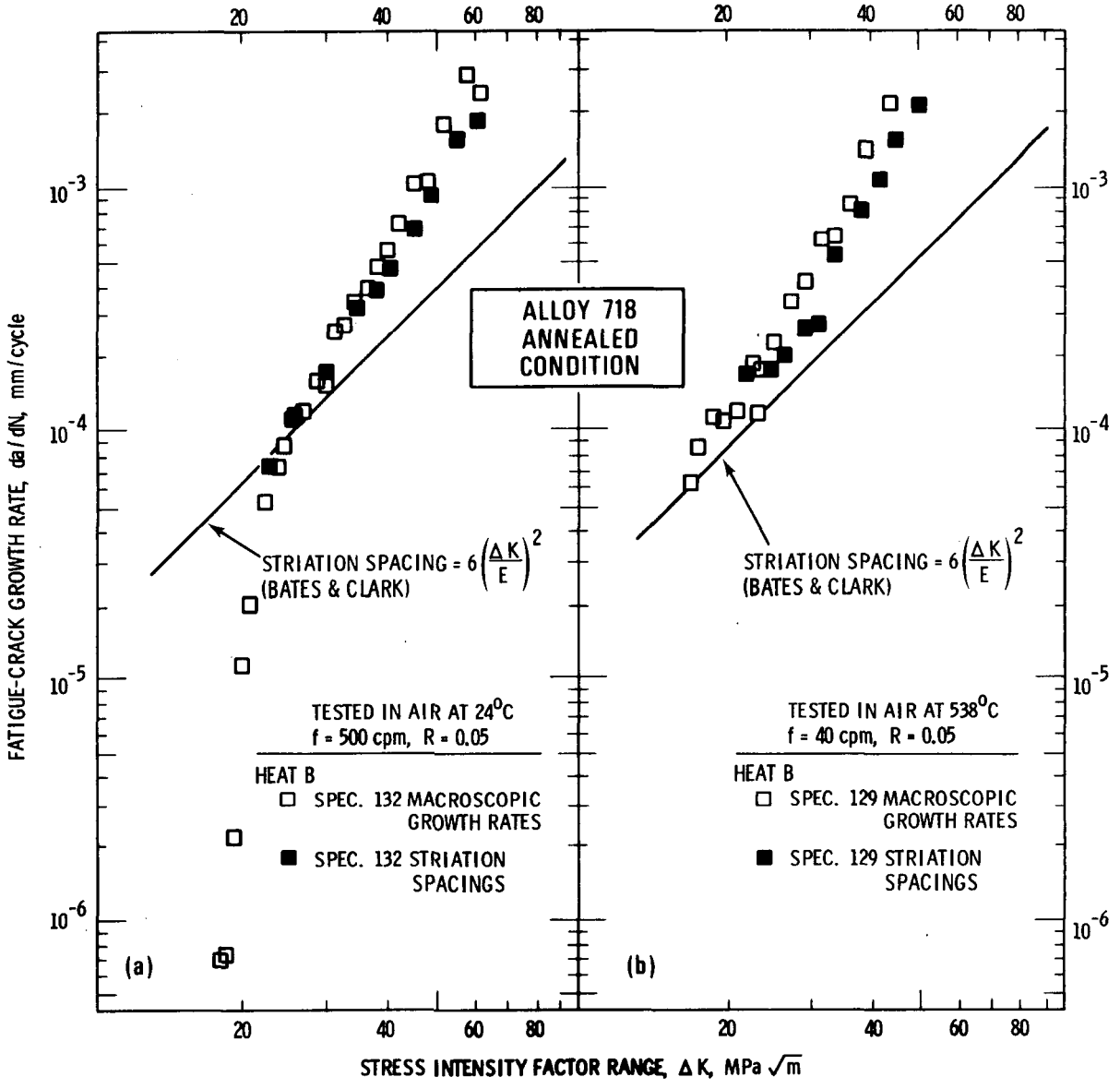

FIGURE 17. Comparison of Striation Spacing Measurements and Macroscopic FCP Rates for Annealed Heat B at (a) Room Temperature and (b) 538°C. Each solid data point represents an average of approximately 110 striation spacing measurements. (Neg. 7903967-1)

IV. CONCLUSIONS

Microstructural aspects of heat-treatment and heat-to-heat variations that influenced the room temperature and elevated temperature fatigue-crack growth behavior of Alloy 718 were characterized in this study. In general, fatigue fracture surface morphologies of conventional, modified, and annealed Alloy 718 were found to be dependent on microstructure, temperature, and stress intensity level as summarized below:

- At intermediate ΔK levels, the room temperature and elevated temperature fracture surfaces for all three heat-treated conditions exhibited a highly striated appearance followed by a combination of striations and microvoids in the highest ΔK regime. Microscopic FCP rates obtained from striation spacing measurements were generally found to be in good agreement with macroscopic crack growth rates, thereby indicating that striation formation controlled the fatigue response of Alloy 718 at intermediate FCP rates.
- Experimentally determined striation spacings in the conventional and modified Alloy 718 conformed to the Bates and Clark empirical relationship between striation spacings and prevailing ΔK levels at 24 and 538°C. In the annealed material, however, striation spacing measurements deviated from the Bates and Clark equation, particularly under higher crack growth rate conditions.
- The acceleration in macroscopic crack growth rates and the generally inferior fatigue resistance exhibited by conventional Heat A in the high FCP regime was associated with the presence of a coarse δ phase network that initiated extensive dimple rupture at high ΔK levels.
- Under low ΔK conditions, the conventional and annealed materials exhibited a cleavage-like, faceted appearance indicative of crystallographic fracture along active slip planes at temperatures up to 538°C. At 24 and 427°C, modified Alloy 718 also exhibited faceting under low stress intensity conditions; however, the facets were not very well defined, since the modified heat-treatment tends to promote homogeneous slip.

- In the 538°C regime, the modified material exhibited extensive intergranular fracture at low stress intensity levels, in contrast to the faceted fracture morphology observed in the conventional and annealed Alloy 718 under comparable test conditions. This behavior is believed to be related to the larger grain size associated with the modified heat-treatment. At 649°C, considerable intergranular cracking was observed in both the conventional and modified conditions.

V. REFERENCES

1. James, L. A. and Mills, W. J., Effect of Heat-Treatment and Heat-To-Heat Variations in the Fatigue-Crack Growth Response of Alloy 718 - Part 1: Macroscopic Observations, Report HEDL-TME 80-9, Hanford Engineering Development Laboratory, Richland, WA, 1980.

2. Mills, W. J., The Influence of Heat Treatment on the Microstructure and Mechanical Properties of Alloy 718 Base Metal and Weldments, Report HEDL-TME 78-54, Hanford Engineering Development Laboratory, Richland, WA, 1978.

3. Smolik, G. R. and Korth, G. E., Reference Heat of Alloy 718 for Department of Energy Programs, Report TREE-1253, EG&G Idaho, Inc., 1978.

4. Bates, R. C. and Clark, W. G., Jr., "Fractography and Fracture Mechanics," Transactions Quarterly, ASM, Vol. 62, pp. 380-389, 1969.

5. Inconel Alloy 718, Huntington Alloy Products Division, The International Nickel Company, Inc., Huntington, WV, 1973.

6. Durquette, D. J. and Gell, M., "The Effect of Environment on the Mechanism of Stage I Fatigue Fracture," Metallurgical Transactions, Vol. 2, pp. 1325-1331, 1971.

7. Gell, M. and Leverant, G. R., "The Characteristics of Stage I Fatigue Fracture in a High-Strength Nickel Alloy," Acta Metallurgica, Vol. 16, pp. 553-561, 1968.

8. Gell, M. and Leverant, G. R., "The Effect of Temperature on Fatigue Fracture in a Directionally-Solidified Nickel-Base Superalloy," Proceedings, 2nd International Conference on Fracture, Brighton, pp. 565-575, 1969.

9. Jablonski, D. A., Carisella, J. V. and Pelloux, R. M., "Fatigue Crack Propagation at Elevated Temperatures in Solid Solution Strengthened Superalloys," Metallurgical Transactions, Vol. 8A, pp. 1893-1900, 1977.

10. Tien, J. K. and Gamble, R. P., "The Room Temperature Fatigue Behavior of Nickel-Base Superalloy Crystals at Ultrasonic Frequency," Metallurgical Transactions, Vol. 2, pp. 1933-1938, 1971.

11. Scarlin, R. B., "Fatigue Crack Propagation in a Directionally-Solidified Nickel-Base Alloy," Metallurgical Transactions, Vol. 7A, pp. 1535-1541, 1976.

12. Moon, D. M. and Sabol, G. P., "Effect of Mean Stress on the High-Cycle Fatigue Behavior of Udimet 700 at 1000°F," Fatigue at Elevated Temperatures, ASTM STP 520, American Society for Testing and Materials, pp. 438-450, 1973.

13. Mills, W. J. and Hertzberg, R. W., "Fatigue Crack Propagation Behavior of the Ni-Ni_3Cb Eutectic Composite," Fatigue of Composite Materials, ASTM STP 569, American Society for Testing and Materials, pp. 5-27, 1975.

14. Clavel, M. and Pineau, A., "Frequency and Wave-Form Effects on the Fatigue Crack Growth Behavior of Alloy 718 at 298K and 823K," Metallurgical Transactions, Vol. 9A, pp. 471-480, 1978.

15. Mills, W. J. and James, L. A., "Effect of Temperature on the Fatigue-Crack Propagation Behavior of Inconel X-750," paper HEDL-SA 1909, Hanford Engineering Development Laboratory, 1979.

16. Mills, W. J. and James, L. A., "Effect of Heat-Treatment on Elevated Temperature Fatigue-Crack Growth Behavior of Two Heats of Alloy 718," ASME Paper 78-WA/PVP-3, New York, December 1978.

17. Smith, H. H. and Michel, D. J., "Fatigue Crack Propagation and Deformation Mode in Alloy 718 at Elevated Temperatures," in Ductility and Toughness Considerations in Elevated Temperature Service, MPC-8, G. V. Smith (Ed.), pp. 225-246, ASME, New York, December 1978.

DISTRIBUTION

UC-79 (137)

UC-79b (38)

UC-79h (31)

DOE/RRT-HQ (2)
Mail Stop B-107
Washington, DC 20545

Program Division Director

DOE/FFTFPO (5)

Director

HEDL (44)

LD Blackburn	W/A-40	WJ Mills (2)	W/A-40
KW Carlson	W/A-40	WE Roake	W/C-16
BA Chin	W/A-58	CT Schaedel	W/A-46
DJ Criswell	W/A-40	LK Severud	W/C-98
AL Dittmer	W/A-40	WF Sheely	W/A-62
AM Ermi	W/A-58	JL Straalsund	W/A-57
EA Evans	W/JAD-6	WD Themar	W/A-40
DS Gelles	W/A-57	AL Ward	W/A-40
DL Greenslade	W/A-40	JA Williams	W/A-40
GW Hollenberg	W/A-59	GL Wire	W/A-58
JJ Holmes	W/A-58	WJS Yang	W/A-57
WL Hu	W/A-58	HH Yoshikawa	W/C-44
LA James (2)	W/A-40	Central Files	(10)
MD Jones	W/A-40	Pub. Services	(2)
RL Knecht	W/A-40	S. Berglin, Contract Administration	W/A-21
GC Massie	W/A-40		
DA Mervyn	W/A-58		